Excitonic and local-field effects in optical spectra from real-space time-domain calculations

W.G. Schmidt, P.H. Hahn and F. Bechstedt

Computational Materials Science Group
Institut für Festkörpertheorie und Theoretische Optik
Friedrich-Schiller-Universität, Max-Wien-Platz 1, 07743 Jena
(Email: W.G.Schmidt@ifto.physik.uni-jena.de)

Abstract. We present a novel approach to solve the Bethe-Salpeter equation for the polarisation function. Rather than from the usual eigenvalue representation, the macroscopic polarisability is obtained from the solution of an initial-value problem. This allows for the first time to calculate excitonic and local-field effects in optical spectra of large and complex systems such as surfaces. As an example we investigate the optical anisotropy of the hydrogen-passivated Si(110) surface. It is shown that the electron-hole attraction is largely responsible for the peculiar line shape of the surface optical spectrum.

1 Introduction

The correct modelling of optical properties has been a long standing issue of scientific interest. It is significant also from a technological point of view, because methods of optical spectroscopy are rapidly gaining importance for materials characterisation. For example techniques like Reflectance Anisotropy/Difference Spectroscopy (RAS/RDS) have evolved from experimental methods to characterise static surfaces to very powerful *in situ* diagnostic probes which allow for the monitoring and controlling of the surface growth in real time and in challenging environments such as in high pressures or under liquids [1]. However, somewhat in contrast to their frequent use, the present understanding of the physical origin of the observed optical phenomena is still rather limited.

Aspnes and Studna [2] discriminated between two components of surface optical spectra: "intrinsic" contributions arising from optical transitions within the bulk and "extrinsic" contributions directly related to the surface chemistry. The latter can often be traced to specific surface electronic states and serve as fingerprints for surface structural motifs [3–5]. The origin of the intrinsic features, however, is harder to explain. It has been discussed for a long time that these features are likely to be related to many-particle effects [6] and/or surface local fields (LF) [7,8], i.e., the influence of the surface-modified microscopic fluctuations of the electric field on the macroscopic dielectric response. However, no definite assignment has been possible yet.

This is largely due to the numerical expense required for converged calculations of surface optical properties. In particular the intrinsic features of the surface spectra are caused by electronic transitions involving a very large number of surface-modified bulk wave functions [3,4]. Therefore, even calculations assuming a single-particle picture for electronic excitations and neglecting self-energy effects are quite involved for surfaces. The inclusion of many-particle effects such as electron-electron and electron-hole interactions dramatically increases the computational cost. Although exact expressions for the excitonic and LF contributions to the surface optical response based on the Bethe-Salpeter equation (BSE) have been derived decades ago, their application has been limited to very few tight-binding (TB) studies [9–11]. Because of the complexity of the problem, another, more frequently used approach approximates LF effects by modelling the crystal surface by a lattice of polarisable entities, which obey a Clausius-Mossotti-like relation [7,8,12]. Obviously, such models as well as TB calculations necessarily depend on external input parameters and cannot account accurately for the surface induced changes of the electronic structure. Very recently, it has become possible to solve the BSE from *first principles* for bulk semiconductors [13,14] and strongly localised surface states [15]. However, the large numerical effort has restricted such calculations to the interaction of relatively few electron-hole pairs. As yet they have not been applied to the surface optical response in a wide spectral range.

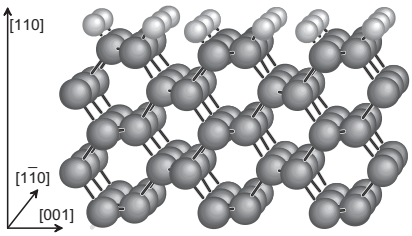

Fig. 1. Upper part of the slab representing the hydrogen-covered Si(110) surface.

Here we use an alternative approach to solve the BSE that allows for the study of large systems such as surfaces. It is shown that many-particle effects on the energies and oscillator strengths of electronic excitations in bulk-like layers are largely responsible for the appearance of the intrinsic features in surface optical spectra. In particular the electron-hole interaction may influence the magnitude and line shape of spectral features.

We use the hydrogen-passivated Si(110) surface (cf. Fig. 1) as a model system. It is one of the first systems studied by RAS [2] and its optical features are mainly intrinsic in character. The passivation of the Si dangling bonds results in there being no surface states in the energy region probed by RAS. The surface spectrum is rather insensitive to the structural and chemical details of the passivation [2,16,17] and has a very characteristic line shape with maxima close to the E_1 and E_2 critical point energies of bulk silicon. Because the RAS spectrum can be easily reproduced, it has become a calibration standard for RAS apparatus and a textbook example for surface optical properties [18].

The physical mechanism leading to the observed line shape, however, is not understood. In their original study [2] Aspnes and Studna argued that the measurements are indicative for the appearance of surface local-fields and/or many-body screening. The strong influence of local fields seems to be supported by model calculations [7,12]. TB studies that neglected LF effects [19] failed to describe the experiment, as did a TB work that included an approximation for LF effects [8]. In the latter study it was concluded that surface defects are responsible for the experimentally observed peaks. While real surface do contain defects, their RAS contributions should be small in that specific case, since the measured spectrum is nearly independent from the surface preparation procedures [2,16,17]. Indeed, a recent *ab initio* calculation [20] that approximated self-energy corrections using a scissors operator, but neglected LF and excitonic effects showed that a hydrogen-terminated Si(110) surface gives rise to optical anisotropies at the bulk critical points without the assumption of surface defects. This work, however, could not account for the peculiar line shape observed experimentally.

We go beyond these previous studies and present a consistent and detailed analysis of how electronic self-energy, LF and excitonic effects manifest themselves in the optical spectrum of Si(110):H. Thereby we proceed in three steps: (i) local density-functional (DFT-LDA) calculations yield the structurally relaxed ground state configuration of the surface, including the Kohn-Sham eigenvalues and eigenfunctions that enter the single- and two-particle Green's functions. (ii) The electronic quasiparticle spectrum is obtained within the GW approximation [21] to the exchange-correlation self-energy and (iii) the BSE is solved for coupled electron-hole excitations [13–15]. Thereby the screened electron-hole attraction and the unscreened electron-hole exchange (cf. Fig. 2) are taken into account [22–24]. Inclusion of the latter allows for a parameter-free calculation of the LF effects. For surfaces LF effects can be expected from both the microscopic fluctuations of the electric field within the bulk, and from the truncation of the bulk itself. The resulting macroscopic polarisabilities are finally used to compute the reflectance anisotropy for normally incident light polarised parallel to the $[1\bar{1}0]$ and [001] directions [25]. The anisotropy of the reflectivity of light polarised in two perpendicular directions in the surface plane, x and y, is given by [25]

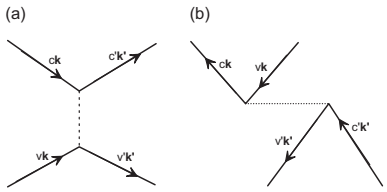

Fig. 2. Schematic representation of electron-hole attraction (a) and electron-hole exchange (b). The screened (unscreened) Coulomb interaction is indicated by a dashed (dotted) line.

$$\frac{\Delta R}{R}(\omega) := 2\frac{R_{xx} - R_{yy}}{R_{xx} + R_{yy}}(\omega) = \frac{16\pi\omega}{c}\Im\left\{\frac{\alpha_{xx}^{hs}(\omega) - \alpha_{yy}^{hs}(\omega)}{\epsilon_b(\omega) - 1}\right\}. \qquad (1)$$

Here $\alpha_{ii}^{hs}(\omega)$ with $i = x, y$ is the diagonal tensor component of the averaged half-slab polarisability and $\epsilon_b(\omega)$ is the bulk dielectric function. Equation 1 contains in principle all contributions to the optical anisotropy such as the ones related to surface electronic states, atomic relaxations, the influence of the surface potential on the bulk wave functions as well as local-field and many-body effects like the electronic self-energy and the electron-hole attraction. Of course, it is not an easy task to include all these contributions in the actual calculations. In the following we discuss our approach to calculate the slab polarisability.

2 Method

2.1 Ground-state calculations within DFT-LDA

We start from *first-principles* pseudopotential calculations, using a massively parallel real-space finite-difference implementation of the DFT-LDA [26], which is characterised by an excellent scaling behaviour on parallel supercomputers such as the Cray T3E [27]. A multigrid technique is used for convergence acceleration. The surface is modeled by periodic supercells containing 12 atomic Si layers (cf. Fig. 1). Silicon dangling bonds at the bottom and top layer are saturated with hydrogen. A vacuum region equivalent to 8 atomic layers in thickness separates the material slabs in [110] direction. Apart from the atoms of the innermost two layers which were kept in their ideal bulk positions, all atomic coordinates are fully relaxed. Four $\mathbf{k}$ points in the irreducible part of the surface Brillouin zone are used for the self-consistent calculation of the ground-state charge density. For the calculation of the surface optical properties we use 140 uniformly distributed $\mathbf{k}$ points.

2.2 Self-energy corrections

When compared quantitatively with experiment, optical spectra calculated within DFT-LDA have serious deficiencies. The most serious one is a systematic redshift of the theoretical features compared to the measurements. This is related to the fact that the quasiparticle character of the electrons, i.e. their mutual interaction and screening is insufficiently accounted for. That leads to an underestimation of the excitation energies known as the DFT-LDA band gap problem [28,29]. In order to include electronic self-energy effects one needs to replace the local exchange and correlation potential $V^{XC}(\mathbf{r})$ in LDA by the nonlocal and energy-dependent self-energy operator $\Sigma(\mathbf{r}, \mathbf{r}'; E)$. The so-called GW approximation (GWA) [30,31] where the self-energy operator is expressed as convolution of the dynamically screened Coulomb potential W and the single-particle propagator G, $\Sigma = iGW$, currently forms the basis of nearly all numerical quasiparticle calculations. Since the calculation of surface optical spectra involves a very large number of electronic states, however, we introduce further approximations. It was found that the real quasiparticle

wave functions have more than 99.9 % overlap with the original DFT-LDA orbitals used as starting point in the calculations, at least for states close to the fundamental band edges of bulk semiconductors [21]. Therefore we obtain the quasiparticle energies ε_n^{QP} from the DFT-LDA eigenvalues and wave functions in a perturbative manner, by

$$\varepsilon_n^{QP}(\mathbf{k}) = \varepsilon_n(\mathbf{k}) + \langle n\mathbf{k}|\Sigma(\varepsilon_n^{QP}) - V^{XC}|n\mathbf{k}\rangle. \tag{2}$$

Here, Σ must in principle be computed self-consistently at the energy ε_n^{QP}. In practice, this is approximated by a Taylor expansion of Σ around the DFT-LDA eigenvalue. To simplify the calculation of the self-energy corrections further, we follow the schemes developed by Hybertsen and Louie [32] and Bechstedt *et al.* [33]: the GW quasiparticle energies are obtained from the DFT-LDA eigenvalues by

$$\varepsilon_n(\mathbf{k})^{QP} = \varepsilon_n(\mathbf{k}) + \frac{1}{1+\beta_{n,\mathbf{k}}}\left[\Sigma^{st}_{n,\mathbf{k}} + \Sigma^{dyn}_{n,\mathbf{k}}\left(\varepsilon_n(\mathbf{k})\right) - V^{XC}_{n,\mathbf{k}}\right], \tag{3}$$

where the self-energy operator Σ has been divided into static and dynamic contributions. Indices at Σ and V^{XC} indicate diagonal matrix elements with the respective wave functions. $\beta_{n,\mathbf{k}}$ is the linear term in the expansion of Σ^{dyn} around the DFT-LDA eigenvalue $\varepsilon_n(\mathbf{k})$. The static part can be further divided into two parts

$$\begin{aligned}\Sigma^{st}(\mathbf{r},\mathbf{r}') = \frac{1}{2}\sum_{n,\mathbf{k}} \psi_{n,\mathbf{k}}(\mathbf{r})\psi^*_{n,\mathbf{k}}(\mathbf{r}')\left[W(\mathbf{r},\mathbf{r}';0) - v(\mathbf{r}-\mathbf{r}')\right] - \\ \sum_{v,\mathbf{k}} \psi_{v,\mathbf{k}}(\mathbf{r})\psi^*_{v,\mathbf{k}}(\mathbf{r}')W(\mathbf{r},\mathbf{r}';0)\ ,\end{aligned} \tag{4}$$

representing the Coulomb hole Σ^{COH} and the screened exchange Σ^{SEX}. The $\psi_{n,\mathbf{k}}$ are the DFT-LDA wave functions. The major bottleneck in the GW calculation is the computation of the screened interaction W. An extreme speedup can be achieved by using a model dielectric function, for which several functional forms have been suggested. We use the version suggested by Bechstedt *et al.* [33]

$$\epsilon(\mathbf{q},\rho) = 1 + \left[(\epsilon_\infty - 1)^{-1} + \left(\frac{q}{q_{TF}(\rho)}\right)^2 + \frac{3q^4}{4k_F^2(\rho)q_{TF}^2(\rho)}\right]^{-1}, \tag{5}$$

where k_F and q_{TF} represent the Fermi and Thomas-Fermi wave-vectors, respectively, which depend on the electron density ρ. This expression interpolates between the correct behaviours at high and low $\mathbf{q}$ vectors and, by construction, correctly obtains the static dielectric constant for $\mathbf{q} = 0$. This simple and intuitive model reproduces very well the RPA results for semiconductors [34]. Together with the LDA-like ansatz of Hybertsen and Louie [32]

for approximating the spatial dependence of the screening of the inhomogeneous system

$$W(\mathbf{r},\mathbf{r}';0) = \frac{1}{2}\left[W^h\left(\mathbf{r}-\mathbf{r}',\rho(\mathbf{r})\right) + W^h\left(\mathbf{r}-\mathbf{r}',\rho(\mathbf{r}')\right)\right] \tag{6}$$

by that of a homogeneous electron gas W^h, (5) allows for an analytic solution for Σ_{COH}. The static Coulomb hole contribution to the self-energy takes the form of a local potential

$$\Sigma^{COH}(\mathbf{r}) = -\frac{q_{TF}(\mathbf{r})}{2}\sqrt{1-\frac{1}{\epsilon_\infty}}\left[1+\frac{q_{TF}(\mathbf{r})}{k_F(\mathbf{r})}\sqrt{\frac{3\epsilon_\infty}{\epsilon_\infty-1}}\right]^{-\frac{1}{2}} , \tag{7}$$

where k_F and q_{TF} are computed for the local density $\rho(\mathbf{r})$.

The matrix elements $\Sigma^{SEX}_{n,\mathbf{k}}$ are calculated in Fourier space. In order to speed up the calculations only the diagonal elements in the Fourier transform of W [32] are retained. The effect of local fields on the screening are approximated by using state-averaged electron densities

$$\rho_{n,\mathbf{k}} = \int d\mathbf{r}^3 \rho(\mathbf{r}) |\psi_{n,\mathbf{k}}(\mathbf{r})|^2 , \tag{8}$$

in the calculation of k_F and q_{TF}. Tests made for bulk Si indicate that rather small deviations, of the order of 0.05 eV, are induced by this approximation. Finally, the dynamic terms $\beta_{n,\mathbf{k}}$ and Σ^{dyn} in (3), are approximated by simple integrals of the dielectric function [33]. For the actual calculations we use (5) together with a single-plasmon-pole approximation to describe the frequency dependence. Local-field effects are again included using the mean-density approximation (8). The integrals are numerically evaluated for a dense sampling of ρ and the results for $\beta_{n,\mathbf{k}}(\rho)$ and $\Sigma^{dyn}(\rho)$ are fitted to polynomials. These are then used for a fast computation of the dynamic contributions to the self-energy during the actual GW calculations.

3 Local fields and electron-hole attraction

The excitation energies obtained within the quasiparticle formalism correctly describe one-particle excitations, such as those involved in (inverse) photoemission experiments. For the description of the optical absorption process, however, one needs to go beyond this single-quasiparticle level. In general, the energy of the absorbed photon differs from the bare, algebraic sum of the hole and electron energies, since the electron-hole interaction also needs to be taken into account. The latter can not only produce absorption below the gap, due to bound exciton states, but can also induce appreciable distortions on the line shape above the continuous absorption edge. The calculation of excitonic effects from *first principles* is only a recent achievement [13,14,36],

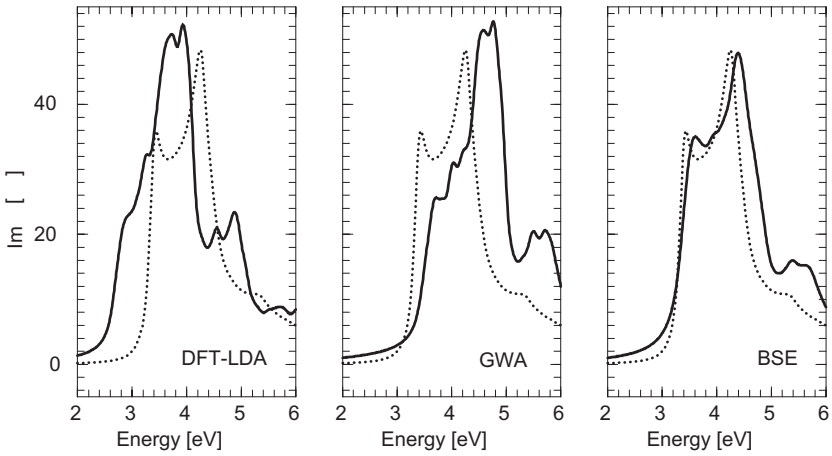

Fig. 3. Dielectric function for bulk Si calculated within DFT-LDA, in GWA and from the BSE (GWA + excitonic and LF effects) in comparison with exp. data from Ref. [35] (dotted line).

and has been restricted to very small systems prior to our work [37]. The polarisation function P including electron-hole attraction and local-field effects can be obtained from the solution of the Bethe-Salpeter equation [22,24],

$$P = P_0 + P_0(\bar{v} - W)P \ , \tag{9}$$

where $\bar{v}$ is the bare Coulomb potential without its long-range part. From the Fourier transform of the diagonal part of P one obtains the macroscopic dielectric function

$$\epsilon^M(\omega) = 1 - \lim_{\mathbf{q}\to 0}\left[v_{00}(\mathbf{q})\int d\mathbf{r}d\mathbf{r}' e^{-i(\mathbf{r}-\mathbf{r}')\mathbf{q}} P(\mathbf{r},\mathbf{r};\mathbf{r}',\mathbf{r}';\omega)\right] . \tag{10}$$

A convenient and natural basis for solving Eq. 9 is given by the orthonormal and complete set of Bloch functions defined, e.g., by the Kohn-Sham problem. Omitting the frequency dependence, the transform of the polarisation into the Bloch-function representation reads

$$P(\mathbf{r}_1,\mathbf{r}_2;\mathbf{r}_3,\mathbf{r}_4) = \sum_{n_1,n_2,n_3,n_4} \psi^*_{n_1}(\mathbf{r}_1)\psi_{n_2}(\mathbf{r}_2)\psi_{n_3}(\mathbf{r}_3)\psi^*_{n_4}(\mathbf{r}_4)P_{(n_1,n_2)(n_3,n_4)}, \tag{11}$$

where n denotes both band index and wave vector. If P_0 is explicitly expressed in terms of Bloch functions and quasiparticle energies, using the Lehmann representation of the single-particle Green's function, and transformed into Bloch space by applying $\int d\mathbf{r}_1 d\mathbf{r}_2 d\mathbf{r}_3 d\mathbf{r}_4 \psi_{n_1}(\mathbf{r}_1)\psi^*_{n_2}(\mathbf{r}_2)\psi^*_{n_3}(\mathbf{r}_3)\psi_{n_4}(\mathbf{r}_4)$, the

solution of the BSE (9) can be written as

$$P_{(n_1,n_2)(n_3,n_4)} = \left[\hat{H} - I\omega\right]^{-1}_{(n_1,n_2)(n_3,n_4)} (f_{n_4} - f_{n_3}), \tag{12}$$

where the two-particle Hamiltonian

$$\begin{aligned}\hat{H}_{(n_1,n_2)(n_3,n_4)} \equiv\ & (\varepsilon^{QP}_{n_1} - \varepsilon^{QP}_{n_2})\delta_{(n_1,n_3)}\delta_{(n_2,n_4)} + (f_{n_2} - f_{n_1})\times \\ & \int d\mathbf{r}_1 d\mathbf{r}_2 d\mathbf{r}_3 d\mathbf{r}_4 \psi_{n_1}(\mathbf{r}_1)\psi^*_{n_2}(\mathbf{r}_2)\psi^*_{n_3}(\mathbf{r}_3)\psi_{n_4}(\mathbf{r}_4)\times \\ & [\delta(\mathbf{r}_1 - \mathbf{r}_2)\delta(\mathbf{r}_3 - \mathbf{r}_4)\bar{v}(\mathbf{r}_1 - \mathbf{r}_3) - \delta(\mathbf{r}_1 - \mathbf{r}_3)\delta(\mathbf{r}_2 - \mathbf{r}_4)W(\mathbf{r}_1, \mathbf{r}_2)]\end{aligned} \tag{13}$$

has been introduced. The $f_n = 0, 1$ is the occupation number of the state n. By performing a matrix inversion for a given frequency ω, the corresponding polarisation is given by Eq. 12. However, for any practical calculation this would be computationally far too expensive, due to the large dimension of $\hat{H}$. This dimension can be reduced by a factor of two, however, if one observes that due to the factors $(f_{n_4} - f_{n_3})$ in (12) and $(f_{n_2} - f_{n_1})$ in Eq. 13, only pairs containing one filled and one empty Bloch state contribute to the macroscopic polarisation. A further reduction of the dimension by a factor of two can be achieved when the off-diagonal blocks coupling the resonant part of $\hat{H}$,

$$\begin{aligned}\hat{H}^{res}_{vc\mathbf{k},v'c'\mathbf{k}'} = & (\varepsilon^{QP}_{c\mathbf{k}} - \varepsilon^{QP}_{v\mathbf{k}})\delta_{vv'}\delta_{cc'}\delta_{\mathbf{k},\mathbf{k}'} + \\ & 2\int d\mathbf{r}_1 d\mathbf{r}_2 \psi^*_{c\mathbf{k}}(\mathbf{r}_1)\psi_{v\mathbf{k}}(\mathbf{r}_1)\bar{v}(\mathbf{r} - \mathbf{r}_2)\psi_{c'\mathbf{k}'}(\mathbf{r}_2)\psi^*_{v'\mathbf{k}'}(\mathbf{r}_2) - \\ & \int d\mathbf{r}_1 d\mathbf{r}_2 \psi^*_{c\mathbf{k}}(\mathbf{r}_1)\psi_{c'\mathbf{k}'}(\mathbf{r}_1)W(\mathbf{r}_1, \mathbf{r}_2)\psi_{v\mathbf{k}}(\mathbf{r}_2)\psi^*_{v'\mathbf{k}'}(\mathbf{r}_2),\end{aligned} \tag{14}$$

and the anti-resonant part, $-\left[\hat{H}^{res}\right]^*$, are neglected. The coupling blocks with contributions only from the interaction terms involving W and $\bar{v}$ are small compared to the (anti-) resonant diagonal blocks containing in addition the quasiparticle transition energies. Apart from special cases, e.g. the calculation of plasmon resonances where the mixing of interband transitions of both positive and negative frequencies must be included in the calculations [38], the coupling can be neglected in the calculation of optical properties [13,39]. Further approximations contained in (14) are the restriction to spin-singlets, static screening and direct transitions, i.e., the neglect of momentum transfer by photons. If furthermore umklapp processes are neglected, the exciton Hamiltonian can be calculated in reciprocal space according to

$$\begin{aligned}\hat{H}^{res}_{vc\mathbf{k},v'c'\mathbf{k}'} = & (\varepsilon^{QP}_{c\mathbf{k}} - \varepsilon^{QP}_{v\mathbf{k}})\delta_{vv'}\delta_{cc'}\delta_{\mathbf{k}\mathbf{k}'} - \\ & \frac{4\pi}{\Omega}\sum_{\mathbf{G},\mathbf{G}'}\{\, 2\frac{\delta_{\mathbf{G}\mathbf{G}'}(1 - \delta_{\mathbf{G}\mathbf{0}})}{|\mathbf{G}|^2} B^{\mathbf{k}\mathbf{k}}_{cv}(\mathbf{G})B^{\mathbf{k}'\mathbf{k}'*}_{c'v'}(\mathbf{G}) -\end{aligned}$$

$$\frac{\epsilon^{-1}(\mathbf{k}-\mathbf{k}'+\mathbf{G},\mathbf{k}-\mathbf{k}'+\mathbf{G}',0)}{|\mathbf{k}-\mathbf{k}'+\mathbf{G}|^2} B^{\mathbf{k}\mathbf{k}'}_{cc'}(\mathbf{G}) B^{\mathbf{k}\mathbf{k}'*}_{vv'}(\mathbf{G}') \Big\}, \tag{15}$$

where the Bloch integral

$$B^{\mathbf{k}\mathbf{k}'}_{nn'}(\mathbf{G}) = \frac{1}{\Omega}\int d\mathbf{r} u^*_{n\mathbf{k}}(\mathbf{r}) e^{i\mathbf{G}\mathbf{r}} u_{n'\mathbf{k}'}(\mathbf{r}) \tag{16}$$

over the periodic parts u of the Bloch wave functions has been introduced. The calculation of the Hamiltonian according to (15) is computationally very demanding even for bulk systems, due to the rank of the Hamiltonian itself, $N = N_v \cdot N_c \cdot N_{\mathbf{k}}$, as well as due to the double sum over $\mathbf{G}$ and $\mathbf{G}'$, which needs to be performed for each single matrix element. In order to speed up the calculations we therefore replace the inverse dielectric matrix by the same diagonal model dielectric function due to Bechstedt (5), which has been used in the calculation of the screened exchange contribution to the self-energy operator. The local-field effects are again approximated by using state-dependent electron densities in (5), which were calculated using the mean-density approximation (8). Despite these simplifications we obtain for bulk Si an optical spectrum in nearly perfect agreement with experiment, as can be seen in Fig. 3. The experimental results are seemingly even better reproduced than in previous calculations [13], where the screening has been fully included. That is simply related to the fact that the approximations included here allow for a better convergence of the technical parameters. The discrepancies between experiment and theory found in Ref. [13,40], for example, are related to the insufficient $\mathbf{k}$-point sampling [41].

After the Hamiltonian has been calculated, one needs to determine the polarisation. The rank of $\hat{H}$ is typically of the order of 10^4 even for small bulk unit cells. This excludes the straightforward evaluation of Eq. 12. The usual approach therefore consists in transforming the inversion into an effective eigenvalue problem, which is then solved by diagonalisation [13,36]. In detail, using the spectral representation

$$\left[\hat{H} - I\omega\right]^{-1} = \sum_{\lambda,\lambda'} \frac{|A^\lambda\rangle S^{-1}_{\lambda,\lambda'} \langle A^{\lambda'}|}{E_\lambda - w}, \tag{17}$$

where $|A^\lambda\rangle$ and E_λ are the eigenvectors and eigenvalues of the exciton Hamiltonian

$$\hat{H}|A^\lambda\rangle = E_\lambda |A^\lambda\rangle \quad \text{and} \quad S_{\lambda,\lambda'} = \langle A^{\lambda'}|A^\lambda\rangle, \tag{18}$$

the ii $(i = x, y, z)$ component of the macroscopic polarisability becomes

$$\alpha^M_{ii}(\omega) = \frac{4e^2\hbar^2}{\Omega} \sum_\lambda \left| \sum_{\mathbf{k}} \sum_{c,v} \frac{\langle c\mathbf{k}|v_i|v\mathbf{k}\rangle}{\varepsilon_c(\mathbf{k}) - \varepsilon_v(\mathbf{k})} A^\lambda_{vc\mathbf{k}} \right|^2 \times \left\{ \frac{1}{E_\lambda - \hbar(\omega+i\eta)} + \frac{1}{E_\lambda + \hbar(\omega+i\eta)} \right\}, \tag{19}$$

where v_i is the corresponding Cartesian component of the single-particle velocity operator. Here, the contributions of the anti-resonant part of the exciton Hamiltonian have been formally included, while the coupling parts are neglected.

The calculation of the dielectric function using (19) is straightforward, but requires the solution of the eigenvalue problem (18). For small bulk unit cells the diagonalisation of $\hat{H}$ can typically be performed within a couple of hours. However, our work aims at the determination of optical properties for large and complex systems such as surfaces. The minimum slab thickness for the calculation of surface optical properties is about 12 layers. Typically more than 100 $\mathbf{k}$ points are needed to sample the surface Brillouin zone. The dimension of the exciton Hamiltonian $N = N_v \cdot N_c \cdot N_{\mathbf{k}}$ is therefore about $10^6 - 10^7$, even for the relatively small unit cell of an unreconstructed surface. Even with today's powerful supercomputers, the diagonalisation of matrices of this size is prohibitively slow. Therefore an approach different from the one outlined above is needed.

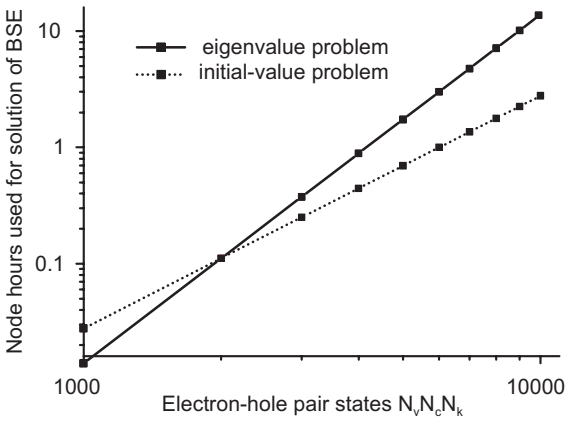

Fig. 4. CPU time needed to solve the BSE on a Pentium PC for bulk Si via an eigenvalue and initial-value problem in dependence on the dimension of the exciton Hamiltonian.

To avoid the diagonalisation bottleneck we exploit an idea by Glutsch *et al.* [42], who traced back a similar eigenvalue problem to an initial-value problem. If a vector $|\mu^i\rangle$ with elements

$$\mu^i_{vc\mathbf{k}} = \frac{\langle c\mathbf{k}|v_i|v\mathbf{k}\rangle}{\varepsilon_c(\mathbf{k}) - \varepsilon_v(\mathbf{k})} \tag{20}$$

is introduced, Eq. 19 takes the form

$$\alpha^M_{ii}(\omega) = \frac{4e^2\hbar^2}{\Omega} \sum_\lambda \left|\langle \mu^i|A^\lambda\rangle\right|^2 \left\{\frac{1}{E_\lambda - \hbar(\omega + i\eta)} + \frac{1}{E_\lambda + \hbar(\omega + i\eta)}\right\}, \tag{21}$$

which is equivalent to

$$\alpha^M_{ii}(\omega) = \frac{4e^2\hbar^2}{\Omega} i \int_0^\infty dt e^{i(\omega+i\eta)t} \left\{\langle \mu^i|\xi(t)\rangle - \langle \mu^i|\xi(t)\rangle^*\right\} \tag{22}$$

with

$$i\hbar\frac{d}{dt}|\xi(t)\rangle = \hat{H}|\xi(t)\rangle \quad \text{and} \quad |\xi(0)\rangle = |\mu^i\rangle. \tag{23}$$

The equivalence can be shown by integrating $|\xi(t)\rangle = e^{\frac{\hat{H}t}{i\hbar}}|\mu\rangle$ and exploiting the spectral representation as in (17). We have also verified numerically that Eqs. 21 and 22 lead to exactly the same spectrum [43]. The latter formula, however, requires much less computational resources. We solve the initial value problem (23) using the central-difference method

$$\hat{H}|\xi(t_{i+1})\rangle = i\hbar\frac{|\xi(t_{i+2})\rangle - |\xi(t_i)\rangle}{2\Delta t}, \tag{24}$$

i.e., by means of a sequence of matrix-vector multiplications. The upper limit of the Fourier integral (22) can be truncated, due to the exponential $e^{-\eta t}$. Therefore, the number of time steps, i.e. matrix-vector multiplications, is nearly independent from the dimension of the system. The operation count for this method scales thus as $\mathcal{O}(N^2)$, compared to the $\mathcal{O}(N^3)$ for the matrix diagonalisation. Moreover, the matrix-vector multiplications can be easily distributed on several processors of a parallel computer, whereas the parallelisation of matrix diagonalisation is less effective, due to the large amount of data transfer across processors. The cross-over point for the CPU time usage of both methods is reached for a number of electron-hole pair states as low as about 2000, as shown in Fig. 4. With the method outline above it is thus possible to include all spectroscopically relevant many-body interactions into calculations of optical properties for systems of an unprecedented size. In the following section we demonstrate the influence of many-body effects on the optical spectrum of the prototypical Si(110):H surface.

4 Results and Discussion

Figure 5 contains the calculated RAS spectra for the Si(110):H surface represented by a 12-layer slab. The DFT-LDA spectrum shows two strong positive RAS features near the E_1 and E_2 bulk critical point energies. However, the features are far too broad. This is partially due to the coarse **k**-point sampling and a slab which is too thin to allow for a complete description of the surface-perturbed bulk wave functions responsible for the observed optical anisotropies. Denser **k**-point meshes and thicker slabs lead to a much better description of the optical anisotropy at the E_2 energy (see Fig. 3 in Ref. [20]). They do not improve the poor representation of the line shape and strength of the anisotropy at the E_1 energy, however. Inclusion of quasiparticle effects in the GWA leads to a blue-shift of the spectrum by about 0.6 - 0.7 eV and changes the line shape. In particular the anisotropy at the E_1 energy is enhanced compared to the DFT-LDA spectrum. The E_1 peak height relative to the E_2 anisotropy is still much smaller than measured, however.

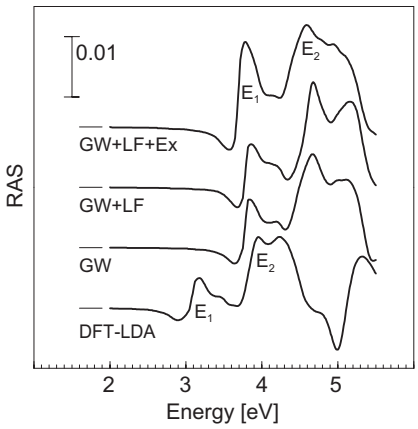

Fig. 5. RAS spectra calculated (within DFT-LDA, in GWA, in GWA with the effects of local fields included, and in GWA with the effects of local fields and the electron-hole attraction included) for Si(110):H described by a 12-layer slab.

In order to determine the influence of excitonic and LF effects on the RAS we calculate the exciton Hamiltonian for the Si(110):H surface according to Eq. 15. In the slab calculation 50 valence and 50 conduction bands at 140 $\mathbf{k}$ points are taken into account. This would give rise to a rank $N = N_v \cdot N_c \cdot N_{\mathbf{k}} = 350,000$ of the exciton Hamiltonian. Fortunately, however, it turns out that not all matrix elements are needed to calculate a numerically converged optical spectrum for the photon energies considered here. By means of a suitable chosen cutoff function we could reduce the rank of the Hamiltonian to about $100,000$. Still, the calculation of 10^{10} matrix elements requires an appreciable amount of computer time, about 15,000 node hours. The task was solved by distributing the calculation on 128 T3E processors. The calculation of the polarisation itself, using the central-difference method (24), is highly efficient. It requires only about $1,500$ node hours.

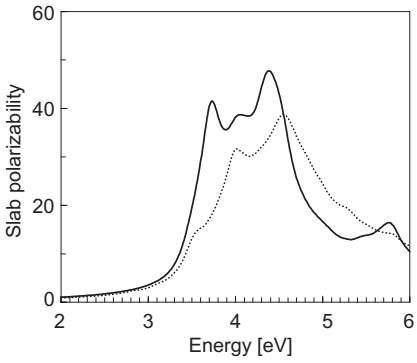

Fig. 6. Imaginary parts of the $\alpha_{[1\bar{1}0]}$ (solid line) and $\alpha_{[001]}$ components (dotted line) of the slab polarisability calculated for Si(110):H in GWA with the effects of local fields and the electron-hole attraction included.

We find that LF effects lead to surprisingly small changes of the spectrum. A reduction of the calculated slab polarisabilities upon inclusion of LF

effects comparable to the one calculated for bulk Si is observed. The reduction acts both on the $\alpha_{[001]}$ and the $\alpha_{[1\bar{1}0]}$ tensor components. It is therefore largely cancelled in the optical anisotropy. Rather than increasing the ratio of the E_1/E_2 peak heights, LF effects even lead to a small decrease. A drastic enhancement of the optical anisotropy at the E_1 energy and a red-shift of the entire spectrum by about $0.1 - 0.2$ eV result, however, from the inclusion of the attractive electron-hole interaction. This is shown by the uppermost spectrum in Fig. 5. Also the characteristic negative anisotropy below the E_1 energy is enhanced by excitonic effects.

Figure 6 shows the calculated slab polarisability. The $[1\bar{1}0]$ component, i.e., the component probed by light with a polarisation direction parallel to the Si-Si zig-zag chains shows a strong peak close to the E_1 energy. On the other hand, the $\alpha_{[001]}$ component has only a weak shoulder at the E_1 energy. This difference is responsible for the strong optical anisotropies measured for passivated Si(110) surfaces.

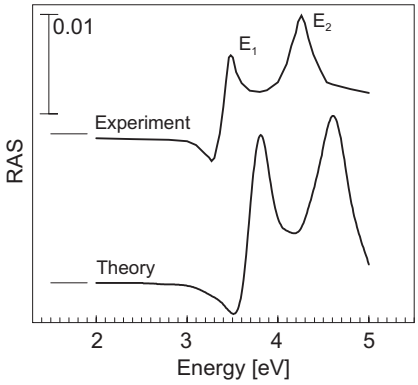

Fig. 7. Measured data for Si(110):H from Ref. [16] are compared with the extrapolation of the 'GW+LF+Ex' curve from Fig. 5 to calculations for a 24-layer slab (see text).

The stepwise inclusion of many-particle effects in the calculation leads to a considerable and systematic improvement of the agreement with the experiment. However, even the uppermost curve in Fig. 5 still deviates from the measured data. On the one hand, this concerns the line shape around the E_2 peak. This is mainly due to the insufficient thickness of our slab. That can be seen from DFT-LDA calculations [20] which are computationally far less expensive and can thus be extended to full numerical convergence. For the comparison with the experimental data [16] shown in Fig. 7 we have therefore extrapolated our calculated spectrum to a thicker slab by adding the difference between the 'GW+LF+Ex' and 'GW' curves from Fig. 5 to the RAS spectrum of Si(110):H calculated in GWA for a 24-layer slab. This simple procedure leads to a rather good description of the measured line shape. However, there remains still another discrepancy between calculation and experiment: the calculated peak positions occur at energies that are about 0.3 eV too

high. Our calculations were performed at the theoretical equilibrium lattice constant of 5.378 Å. That leads to an increase of the energy splitting between occupied and empty states by about 0.1 eV compared to calculations at the experimental lattice constant. Temperature effects in the measured spectra which are neglected in our calculations result in a red-shift of the optical spectra by a similar amount [44]. The remaining difference to the experiment is related to numerical insufficiencies as the relatively small number of $\mathbf{k}$ points and our approximations in calculating the screened Coulomb potential W. The latter tend to lead to slightly overestimated excitation energies [33].

5 Summary

In summary, we have demonstrated that by using a time-evolution rather than a matrix-diagonalisation technique for the solution of the Bethe-Salpeter equation, it is now possible to include excitonic and local-field effects in the calculation of optical properties of complex systems consisting of many atoms. We calculated the optical anisotropy of the prototypical Si(110):H surface, the origin of which has been the subject of a long-standing controversy. It is shown that excitonic effects via strong modifications of the optical response of surface-modified bulk wave functions determine largely the line shape of the optical features. Local-field effects are found to play a much smaller role than previously thought. We expect the method presented here to be extremely useful for the accurate calculation of optical properties for many more systems characterised by a large number of electron-hole pairs.

We thank S. Glutsch, L. Reining and V. Olevano for very helpful discussions. Grants of computer time from the Höchstleistungsrechenzentrum Stuttgart are gratefully acknowledged.

References

1. D. E. Aspnes, Solid State Commun. **101**, 85 (1997).
2. D. E. Aspnes and A. A. Studna, Phys. Rev. Lett. **54**, 1956 (1985).
3. W. G. Schmidt, N. Esser, A. M. Frisch, P. Vogt, J. Bernholc, F. Bechstedt, M. Zorn, T. Hannappel, S. Visbeck, F. Willig, and W. Richter, Phys. Rev. B. **61**, R16335 (2000).
4. W. G. Schmidt, F. Bechstedt, and J. Bernholc, J. Vac. Sci. Technol. B **18**, 2215 (2000).
5. W. Lu, W. G. Schmidt, E. L. Briggs, and J. Bernholc, Phys. Rev. Lett. **85**, 4381 (2000).
6. L. Mantese, K. A. Bell, D. E. Aspnes, and U. Rossow, Phys. Lett. A **253**, 93 (1999).
7. W. L. Mochán and R. G. Barrera, Phys. Rev. Lett. **55**, 1192 (1985).
8. B. S. Mendoza, R. Del Sole, and A. I. Shkrebtii, Phys. Rev. B **57**, R12709 (1998).
9. C. H. Wu and W. Hanke, Solid State Commun. **23**, 829 (1977).

10. R. Del Sole and E. Fiorino, Phys. Rev. B **29**, 4631 (1984).
11. R. Del Sole and A. Selloni, Phys. Rev. B **30**, 883 (1984).
12. B. S. Mendoza and W. L. Mochán, Phys. Rev. B **55**, 2489 (1997).
13. S. Albrecht, L. Reining, R. Del Sole, and G. Onida, Phys. Rev. Lett. **80**, 4510 (1998).
14. L. X. Benedict, E. L. Shirley, and R. B. Bohn, Phys. Rev. Lett. **80**, 4514 (1998).
15. M. Rohlfing and S. G. Louie, Phys. Rev. Lett. **83**, 856 (1999).
16. T. Yasuda, D. E. Aspnes, D. R. Lee, C. H. Bjorkman, and G. Lucovsky, J. Vac. Sci. Technol. A **12**, 1152 (1994).
17. K. Hingerl, R. E. Balderas-Navarro, A. Bonanni, P. Tichopadek, and W. Schmidt, Appl. Surf. Sci. **175/176**, 769 (2001).
18. P. Y. Yu and M. Cardona, *Fundamentals of Semiconductors* (Springer-Verlag, Berlin, 1999).
19. A. Selloni, P. Marsella, and R. Del Sole, Phys. Rev. B **33**, 8885 (1986).
20. W. G. Schmidt and J. Bernholc, Phys. Rev. B **61**, 7604 (2000).
21. M. S. Hybertsen and S. G. Louie, Phys. Rev. B **34**, 5390 (1986).
22. L. J. Sham and T. M. Rice, Phys. Rev. **144**, 708 (1966).
23. W. Hanke and L. J. Sham, Phys. Rev. B **12**, 4501 (1975).
24. W. Hanke and L. J. Sham, Phys. Rev. B **21**, 4656 (1980).
25. R. Del Sole, Solid State Commun. **37**, 537 (1981).
26. J. Bernholc, E. L. Briggs, C. Bungaro, M. B. Nardelli, J. L. Fattebert, K. Rapcewicz, C. Roland, W. G. Schmidt, and Q. Zhao, phys. stat. sol. (b) **217**, 685 (2000).
27. W. G. Schmidt, P. H. Hahn, and F. Bechstedt, in *High Performance Computing in Science and Engineering 2001*, p. 178 (Springer-Verlag, Berlin, 2002).
28. F. Aryasetiawan and O. Gunnarsson, Rep. Prog. Phys. **61**, 237 (1998).
29. F. Bechstedt, in *Festköperprobleme / Advances in Solid State Physics*, edited by U. Rössler (Vieweg, Braunschweig/Wiesbaden, 1992), Vol. 32, p. 161.
30. L. Hedin, Phys. Rev. **139**, A769 (1965).
31. L. Hedin and S. Lundqvist, in *Solid State Physics*, edited by H. Ehrenreich, F. Seitz, and D. Turnball (Academic, New York, 1969), Vol. 23, p. 1.
32. M. S. Hybertsen and S. G. Louie, Phys. Rev. B **37**, 2733 (1988).
33. F. Bechstedt, R. Del Sole, G. Cappellini, and L. Reining, Solid State Commun. **84**, 765 (1992).
34. G. Cappellini, R. Del Sole, L. Reining, and F. Bechstedt, Phys. Rev. B **47**, 9892 (1993).
35. D. E. Aspnes and A. A. Studna, Phys. Rev. B **27**, 985 (1983).
36. M. Rohlfing and S. G. Louie, Phys. Rev. Lett. **80**, 3320 (1998).
37. P. H. Hahn, W. G. Schmidt, and F. Bechstedt, Phys. Rev. Lett. **88**, 016402 (2002).
38. V. Olevano and L. Reining, Phys. Rev. Lett. **86**, 5962 (2001).
39. S. Albrecht, Ph.D. thesis, École Polytechnique, Paris, 1999.
40. M. Cardona, L. F. Lastras-Martinez, and D. E. Aspnes, Phys. Rev. Lett. **83**, 3970 (1999).
41. S. Albrecht, L. Reining, G. Onida, V. Olevano, and R. Del Sole, Phys. Rev. Lett. **83**, 3971 (1999).
42. S. Glutsch, D. S. Chemla, and F. Bechstedt, Phys. Rev. B **54**, 11592 (1996).
43. P. H. Hahn, Master's thesis, Friedrich-Schiller-Universität Jena, 2001.
44. P. Lautenschlager, M. Garriga, L. Viña, and M. Cardona, Phys. Rev. B **36**, 4821 (1987).